Molecular dynamics study of diffusion of xenon in water at different temperatures

Niraj Kumar Nepal[1] and Narayan Prasad Adhikari[1]

[1]Central Department of Physics, Tribhuavn University, Kirtipur, Kathmandu, Nepal

Abstract

Molecular Dynamics simulation was performed using 2 xenon atoms as solute and 300 water molecules as solvent. We have studied the structural properties as well as transport property. As structural properties, we have determined the radial distribution function (RDF) of xenon-xenon, xenon-water, and water-water interactions. Study of RDF of xenon-xenon and oxygen-oxygen interactions of water shows that there is hydrophobic behavior of xenon in the presence of water. We have studied the self diffusion coefficient of xenon, water, and mutual diffusion coefficients of xenon in water. The self diffusion coefficient of xenon was estimated using both mean-squared displacement (MSD) and velocity autocorrelation function (VACF), while only MSD was used for water. The temperature dependence of the diffusion coefficient of xenon and water were found to follow the Arrhenius behavior. The activation energies obtained are 12.156 KJ/mole with MSD and 14.617 KJ/mole with VACF in the temperature range taken in this study.

Index Terms: molecular dynamics, xenon, water, diffusion coefficient, hydrophobic interactions

1. Introduction

Water, the most essential component of the nature forms the basic building block of every living and nonliving things, and takes part in almost all natural phenomena. The strong hydrogen bonding between water molecules is responsible for many unusual phenomena where water is a solvent. The noble gases are uncharged and monoatomic particles, and cannot participate in hydrogen bonding. The presence of noble gases in water exhibits a number of uncommon features related to hydration of these gases through the hydrophobic interaction. The transport property such as diffusion of such gases always is of particular interest. We intend to study the different properties of xenon in the presence of water.

Several experimental and theoretical studies have been performed in the past to study the hydrophobic interaction[1] and to estimate the diffusion coefficient of xenon in water.[2-6] However, special consideration is given to the estimation of the diffusion coefficient in this study. There are different methods to estimate the diffusion coefficient. Electron-Spin Resonance (ESR), Dynamic Light Scattering (DLS), and Nuclear Magnetic Resonance (NMR) are some famous techniques which enable us to study the diffusion coefficient.[7] Alternatively, we can estimate the diffusion coefficient by using molecular dynamics (MD) as it provides an opportunity to track the coordinates of all the particles in the system.

MD simulation can be used to study the transport and mechanical properties of complex systems at an atomic level by following the dynamic motion of the particles within the system.[8] Complex systems include biologically operated systems in life, such as the folding of proteins and nucleic acids (adopting specific structures consistent with their function), transportation of ions through membranes, the triggering of series of chemical reactions by enzymes, diffusion of nutrition in hemoglobin, etc.

The organization of the paper is as follows. We present the underlying theory and computational method in Section 2 and Section 3 respectively, while we will discuss our results in Section 4,

and finally, we will conclude the discussion in Section 5.

2. Theory

2.1 Fick's Law and Einstein's Relation
When mass, energy or momentum is transferred through a system, the transport is described to first order by a phenomenological relation of the form,[9]

$$\mathbf{J} = \text{- coefficient} * \text{gradient} \qquad (1)$$

The flux **J** measures the transfer per unit area in unit time, the gradient provides the driving force for the flux and the coefficient characterizes the resistance to flow. In the case of diffusion, which is the transport of mass, this phenomenological relation leads to Fick's Law,

$$\mathbf{J} = -D\nabla C(r, t) \qquad (2)$$

The vector of the diffusion flux **J** is directed oppositely in direction to the concentration gradient vector ∇C. The concentration gradient vector always points in that direction for which the concentration field undergoes the most rapid increase, and its magnitude equals the maximum rate of concentration at the point. For an isotropic medium the diffusion flux is antiparallel to the concentration gradient. The diffusion flux is expressed in number of particles (or moles) traversing a unit area per unit time and the concentration in number of particles per unit volume. Thus, the diffusivity D has the dimension of length*length per unit time and has the unit $[cm^2 s^{-1}]$ or $[m^2 s^{-1}]$.[10]

For a diffusing species which obeys a conservation law an equation of continuity can be formulated.

$$\frac{\partial C(r,t)}{\partial t} + \nabla . \mathbf{J}(r, t) = 0 \qquad (3)$$

Equation 3 is the continuity equation. Using *Equation 2* and *Equation 3*, one gets[11]

$$D(t) = \frac{1}{6}\frac{\partial}{\partial t} < r^2(t) > \qquad (4)$$

Equation 4 is the famous Einstein relation which relates the diffusion coefficient, a macroscopic transport property of the system, with the mean-squared displacement, a microscopic quantity of the diffusing particles of the system.[11] As in *Equation 4*, the instantaneous value of the diffusion coefficient can be obtained from the slope of the MSD curve with time. For an MSD that behaves as a straight line after a prolonged period of time, *Equation 4* reduces to

$$D = \lim_{t \to \infty} \frac{<r^2(t)>}{6t} \qquad (5)$$

This shows that by tracking the coordinates and hence the position of each particle all the time we can calculate the diffusion coefficient.

2.2. Green-Kubo Formalism (Velocity Auto Correlation Function)
The Green-Kubo formalism relates macroscopic properties (e.g. the diffusion coefficient, in particular a response property of the system) to microscopic properties (fluctuations of the equilibrium distribution). The diffusion coefficient is a response property of the system to a concentration inhomogeneity. The velocity auto-correlation function is an equilibrium property of the system, because it describes the correlations between velocities at different times along an equilibrium trajectory.[11]

$$D = \frac{1}{3}\int_0^\infty d\tau < v_x(\tau)v_x(0) > \qquad (6)$$

The ensemble average term in *Equation 6* is the velocity auto-correlation function.

3. Computational Details
The simulation has been carried out using the molecular dynamics simulation package GROMACS 4.6.1 (GROningen MAchine for Chemical Simulation) with GROMOS force field.[13] The system consists of 2 xenon atoms as solute and 300 water molecules as solvent. The first step to start the simulation is to model the system, which is discussed as follows.

3.1 Modeling of xenon and water

Modeling of the system is done by taking the potential energy as a reference. The total potential energy is a combination of different bonded and non-bonded interactions. Bonded interactions include bond stretching, bond-angle vibration, proper dihedral, and improper dihedral. The non-bonded interactions include van der Waals interactions and coulomb interactions. As xenon is a monoatomic noble gas, only contributions from the van der Waals interaction are taken. The non-bonded interactions (van der Waals interactions) between the diffusing particles have been approximated by the Lennard-Jones potential,

$$U_{LJ}(r_{ij}) = 4\epsilon_{ij}[\left(\frac{\sigma_{ij}}{r_{ij}}\right)^{12} - \left(\frac{\sigma_{ij}}{r_{ij}}\right)^{6}] \qquad (7)$$

where, r_{ij} is the distance between two particles i and j, $2^{(1/6)}\sigma$ is the equilibrium distance between the two particles, and ϵ_{ij} is the strength of the interaction. The GROMACS *Equation 7* is modified as,[13]

$$U(r_{ij}) = \frac{C_{12}}{r_{ij}^{12}} - \frac{C_6}{r_{ij}^6} \qquad (8)$$

where parameters $C_{12}= 4\epsilon_{ij}\sigma^{12}$ and $C_6= 4\epsilon_{ij}\sigma^6$ depends on pair of atom types.

The flexible SPC/E model of water has been used in the present study. It is a semi-empirical model, consisting of three point charges on each atomic site, two in the hydrogen atom and one in the oxygen atom. The values of σ and ε are presented in *Table 1*. Furthermore, hydrogen and oxygen carry certain charges in a water molecule.

Table 1. L-J Parameters for Xenon[12] and water.[13-15]

Molecule	σ (nm)	ε (K)
Xe	0.39011	227.55 k_B
Water	0.316565	78.197 k_B

Each Hydrogen atom carries a partial charge of +0.4238e, and oxygen atom carries a partial charge of −0.847e where "e" is the elementary charge having magnitude 1.6022×10^{-19}C. In this model the intramolecular potential consists of a harmonic bond and angle vibration terms.

$$U_{OH}(r) = \frac{1}{2}\sum K_{OH}(r - b_{OH})^2 \qquad (9)$$

and

$$U_{OH}(\theta) = \frac{1}{2}K_{HOH}(\theta - \theta_o)^2 \qquad (10)$$

where K_{OH} is the spring constant which measures the strength of the interatomic bond between an oxygen and hydrogen atom; b_{OH} is the equilibrium bond length between oxygen and hydrogen atoms. Similarly, K_{HOH} is the spring constant for bond angle vibration with θ_o as the equilibrium H-O-H bond angle. The parameters that were used for our study are listed in the *Table 2*. These parameters were presented in the file named spce.itp attached to GROMACS.

Table 2. Intramolecular potential parameters for the flexible SPC/E model of water.[13-15]

Parameters	Values
K_{OH}	$3.45X10^{+05}$ KJ $mol^{-1}\,nm^{12}$
b_{OH}	0.1 nm
K_{HOH}	$3.83X10^{+02}$ KJ $mol^{-1}\,rad^{-2}$
$\Theta\circ$	109.47∘

The Lennard-Jones non-bonded parameters for the SPC/E water model are given in *Table 2*. The parameters for the xenon-water interaction are obtained by using the Lorentz-Bertholet combination rule:

$$\epsilon = \sqrt{\epsilon_{Xe}\epsilon_{water}} \quad ; \quad \sigma = \frac{1}{2}(\sigma_{Xe} + \sigma_{water}).$$

The solution is prepared by using xenon as a solute and water as a solvent with mole fractions of 0.0066 and 0.9934 respectively. The simulation was carried out in a cubic box with dimensions of 2.8 nm shown as in *Figure 1*. As atoms in water have partial charge, the non-

bonded interaction also includes the Coulomb interaction between the oxygen and hydrogen atoms of two different water molecules, as given by Coulomb's law.
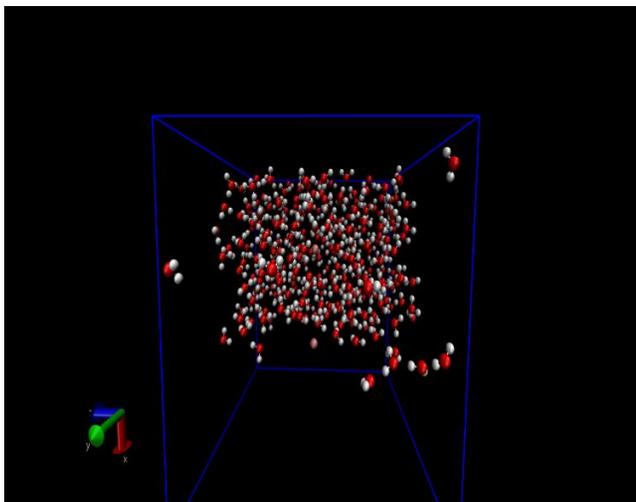

Figure 1. Structure of the system before energy minimization .[16]

3.2 Energy minimization

After solvation, energy minimization is carried out. Energy minimization removes bad contacts between different particles in the system, reduces thermal noise in the structure and brings the system to one of the local minima. The steepest descent algorithm has been used for energy minimization. ***Figure 2*** represents the structure and potential energy versus time plot after energy minimization.

3.3 Equilibration Run

Energy minimization is followed by an equilibration run of 100 ns subjected to NPT ensemble which ensures that the temperature, pressure, and density of the system are fixed at the desired values. This is done to achieve thermodynamic equilibrium, as the dynamic properties like diffusion vary with these parameters. The number of particles within the system is kept fixed by using periodic boundary conditions, where we create replicas of the system (supercell) surrounding the system under study. If a particle leaves the supercell, an exact image enters the supercell from a neighboring replica, keeping the particle number constant. Temperature coupling and pressure coupling are done by velocity-rescale thermostat and Berendsen thermostat respectively. The leap-frog algorithm has been used as an integrator and all bonds are converted to constraints using the SHAKE algorithm. ***Table 3*** lists the temperatures and densities of the system obtained after the equilibration process was carried out for the system structure after energy minimization.
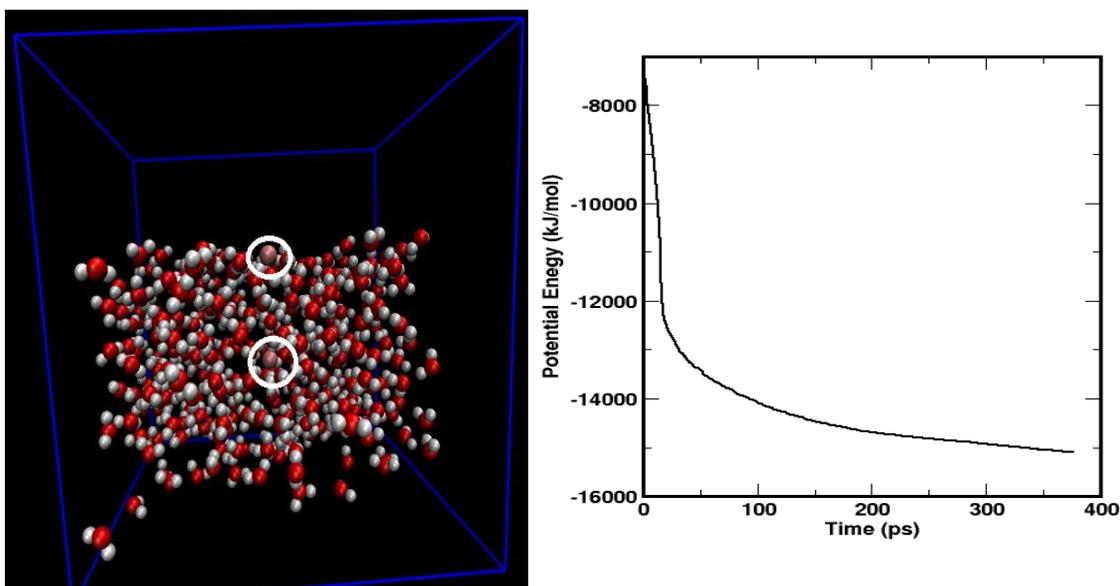

Figure 2. Structure and potential energy of the system after energy minimization. Right panel shows the potential energy as a function of time.

3.4 Production Run
Equilibration is followed by a production run (a final step to calculate the desired dynamic property-diffusion coefficient) where we fix the system volume. So, the system is now an NVT ensemble. A production run is carried out for 200 ns. Pressure coupling is eliminated to ensure it is an NVT ensemble.

Table 3. Values of the simulated temperature (Tsim) and density ρ of the system at various coupling temperatures (T). ρ is the density of the system under study. From **Table 3**, we see that the density of the system at all the temperatures is found to be close to the density of water, ensuring the validity of the force field parameters we used in the present work.

Temperature (K)	$T_{simulation}$ (K)	Density (Kg/m^3)
303	302.943 ± 0.011	1021.42 ± 0.21
313	312.959 ± 0.013	1015.38 ± 0.14
323	322.952 ± 0.018	1008.51 ± 0.12
333	332.970 ± 0.030	1001.09 ± 0.16

4. Structural Analysis
The structural analysis of the system is performed through the Radial Distribution Function (RDF). In the oxygen-oxygen radial distribution function ($g_{OW-OW}(r)$), OW represents the oxygen atom of the water molecule. The xenon-oxygen radial distribution function ($g_{Xe-OW}(r)$), and xenon-xenon radial distribution function ($g_{Xe-Xe}(r)$) have already been discussed.

4.1 RDF of oxygen-oxygen in water
Figure 3 (left) presents the radial distribution function of oxygen-oxygen in water molecules at different temperatures. The value of $g_{OW-OW}(r)$ is zero up to the certain radial distance from the origin and after that it starts to increase. The region from the origin up to which the value of $g_{OW-OW}(r)$ is zero is called exclusion region. The value of $g_{OW-OW}(r)$ is maximum at a certain radial distance, that point is called the first peak point and corresponding value is the first peak value. The rise and fall in the value of $g_{OW-OW}(r)$ can be seen in **Figure 3**, giving rise to a second and third peak value. After the third peak, it becomes almost constant. As the peak value decreases and minimum value increases with increasing radial distance and finally becomes constant later. The different peak values with the corresponding points are tabulated in **Table 4**.

From **Table 4**, it can be seen that the excluded region of OW-OW interaction lies within 0.247 nm at 303 K, which is less than that of van der Waals radius (0.355 nm) of the oxygen-oxygen interaction. The size of the excluded region seems to be decreasing with increasing temperature. The random motion of the particles increases with an increase in temperature due to thermal agitation. This may increase the probability that the particle comes closer to another particle in spite of its van der Waals interaction range.
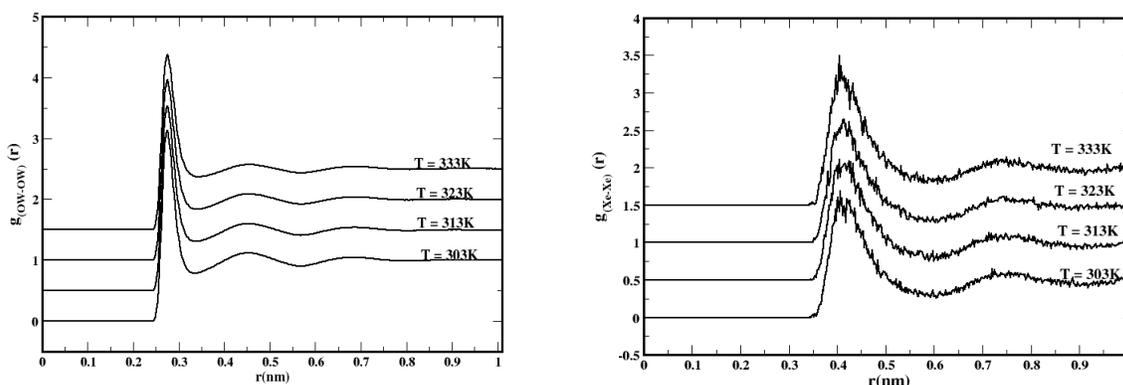

Figure 3. Radial distribution functions, $g_{OW-OW}(r)$ (left) and $g_{Xe-Xe}(r)$ (right) at different temperatures and densities. The RDF at temperatures 313 K, 323 K, and 333 K have been shifted by 0.5, 1.0, and 1.5 respectively along y-axis.

Table 4. RDF, $g_{OW-OW}(r)$, of solvent at different temperatures and different densities. ER: Excluded Region FPP: First Peak Position — FPV: First Peak Value SPP: Second Peak Position — SPV: Second Peak Value TPP: Third Peak Position — TPV: Third Peak Value FMP: First Minimum Position — FMV: First Minimum Value SMP: Second Minimum Position — SMV: Second Minimum Value.

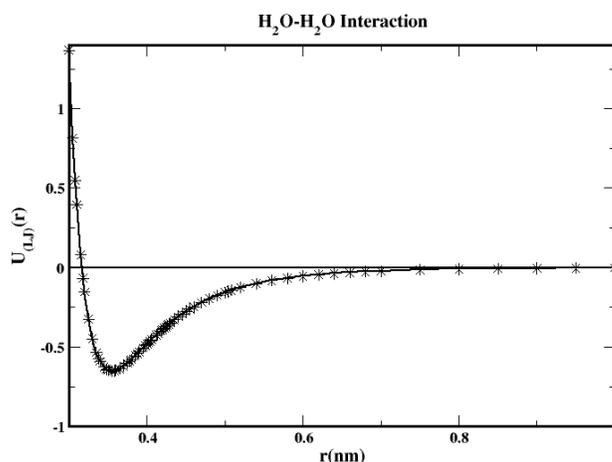| Temperature (K)	ER (nm)	FPP (nm)	FPV	SPP (nm)	SPV	TPP (nm)	TPV	FMP (nm)	FMV	SMP (nm)	SMV
303	0.247	0.276	3.102	0.451	1.104	0.687	1.033	0.340	0.775	0.571	0.902
313	0.246	0.276	3.006	0.453	1.083	0.688	1.027	0.340	0.806	0.571	0.908
323	0.244	0.278	2.933	0.455	1.074	0.688	1.027	0.345	0.827	0.571	0.919
333	0.244	0.278	2.849	0.457	1.058	0.690	1.022	0.346	0.867	0.572	0.931

Figure 4. Plot of Lennard-Jones potential as a function of distance for two water molecules.

The first peak values lie within 0.28 nm, which is also less than that of van der Waals radius with a corresponding peak value of about 3.1. This means other potentials along with the Lennard-Jones potential also play a role as seen in ***Figure 4***. In ***Figure 3***, we see that the maximum probability of finding oxygen atoms from other water molecules with respect to a fixed oxygen atom shift left when we consider both the Lennard-Jones and Coulomb potentials acting on the particle compared to when we consider the Lennard-Jones interaction only. Here we consider only two water molecules to get the combined Lennard-Jones and Coulomb potential, as it is difficult to analysis the many body effect on the combined potential. The result we get is consistent with ***Table 4***, where the FPP is less than the van der Waals radius.

Table 4 shows that the peak values decrease with increasing temperature and also the first peak point is shifted to right as the temperature is raised. It can also be seen that the first minimum point increases and the exclusion region decreases with increasing temperature. This will increase the width of the peak as the temperature is raised. The decrease in height and increase in width of the first peak of $g_{(OW-OW}(r))$ point to a change in the nearest neighbor coordination number[1] which indicates that the solvent becomes less structured as the temperature increases. Similarly, the second and third peak points and corresponding values show similar results to that of first peak.

4.2 RDF of xenon-xenon interaction
Figure 3 (right) is the radial distribution function of xenon $g_{(Xe-Xe}(r))$ at different temperatures. Also the Van der Waals radius of xenon is 0.438 nm for the system under study. As is seen from ***Figure 3*** (right), the excluded regions for xenon atoms lie within 0.345 nm, where $g_{(Xe-Xe}(r))$ is zero, as it is less than the van der Waals radius of

xenon. There are no atoms present within this region.

The roughness in the figure is due to insufficient statistics caused by the small number of xenon atoms. The first peak occurs around 0.42 nm, where the probability of finding xenon atoms is a maximum. The distance at which the first peak occurs is called nearest neighbor separation, which is less than the van der Waals radius, which may be due to the tendency of noble gas to aggregate in the presence of water. The second peak occurs at around 0.76 nm. Further the presence of the first and second peaks signifies that the xenon atoms do not move independently but are correlated to some extent though small in number.

As can be seen from *Figure 3* (right), the gap between two successive peaks is increasing with increase in temperature. This is opposite to the case of the oxygen-oxygen interaction within water, where these peak values decrease with increasing temperature. This means that the xenon atoms tend to aggregate with increasing temperature. However, the oxygen atoms of the water molecules move away from each other with increasing temperature. The unusual thermo-physical properties of dilute solutions of nonpolar substances in water are usually explained as "hydrophobic interactions" - special interactions between two or more nonpolar solute molecules in water, solute interactions with water molecules, and interactions between water molecules in the vicinity of these solutes.

4.3 RDF of xenon-oxygen interaction
The radial distribution function of solvent with respect to xenon atoms, $g_{Xe-OW}(r)$, in the system at different temperatures and corresponding system densities have been studied. The plot of RDF at different temperatures is shown in *Figure 5*. The excluded regions remain confined within 0.305 nm, which is less than the Van der Waals radius 0.397 nm of the xenon-water interaction. The position of the first peaks is fixed at around 0.381 nm. The first peak value decreases with a rise in temperature by small amounts for the first parameter and also for the second parameter except at 323 K. The second peaks also seem to be fixed at 0.666 nm. Moreover, the widths of the peaks increase with the increase in temperature. This signifies that the correlation between the xenon and solvent molecules decreases as temperature is increased, which is due to the thermal energy acquired by them as it is proportional to temperature. *Table 5* gives the details of the radial distribution function of the solvent molecules with respect to the xenon atoms.

Table 5. RDF, gXe−OW(r), of solute-solvent at different temperatures and different densities.

Temperature (K)	ER (nm)	FPP (nm)	FPV	SPP (nm)	SPV	FMP (nm)	FMV	SMP (nm)	SMV
303	0.306	0.381	1.951	0.666	1.093	0.555	0.744	0.926	0.979
313	0.307	0.381	1.901	0.666	1.073	0.555	0.758	0.926	0.979
323	0.305	0.381	1.878	0.666	1.069	0.555	0.768	0.926	0.982
333	0.305	0.381	1.871	0.668	1.073	0.555	0.772	0.926	0.986

4.4 Self-Diffusion Coefficient
The self diffusion coefficient is obtained through the Mean Square Displacement (MSD) method and the Velocity autocorrelation (VACF) method. *Figure 6* presents the plot of the MSD vs time at different temperatures. Although the production run for the NVT ensemble is 200 ns, we have truncated the MSD versus time graph to 2 ns for better statistics. The slope of this graph divided by 6 gives the self-diffusion coefficient. The graph shows that the MSD varies linearly with time as expected. The MSD increases with the temperature, indicating that the diffusion coefficient increases with increasing temperature. This is because with an increase in temperature the density of system decreases, thereby increasing the space available for xenon atoms to execute a random walk. The self diffusion

coefficient is estimated after the system attains the equilibrium state, i.e. has zero concentration gradient, which can be illustrated by using a logarithmic plot of the MSD vs time and a plot of the diffusion coefficient vs time.
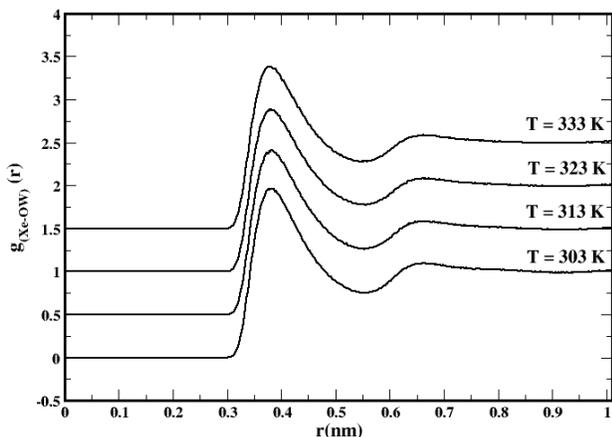

Figure 5. Radial distribution function, $g_{Xe-OW}(r)$, at different temperatures and corresponding densities. The RDF at temperatures 313 K, 323 K, and 333 K have been shifted by 0.5, 1.0, and 1.5 respectively along y-axis.

In the logarithmic plot of the MSD vs time, it can be seen that the MSD follows a parabolic profile, which can be explained by using the diffusion coefficient vs time plot. This shows that diffusion coefficient is high at first which is due to the ballistic motion of xenon atoms, then, after a certain time, the graph is almost constant, showing that the system is in an equilibrium state. *Figure 7* shows the variation of the velocity-autocorrelation function with time at 303K. The values of the diffusion coefficient of xenon obtained by using the two approaches, namely the MSD and VACF, at different temperatures is tabulated in *Table 6*. The self diffusion coefficient increases with an increase in temperature, as expected. This is because of the increase in velocity of the xenon atoms in accordance with the increase in temperature. Also, the density of the system decreases and the space available for the xenon atoms to execute random walk motion increases. Similarly, the self diffusion of water has been discussed. The value of the self diffusion coefficient of water with respect to xenon has been compared to the experimental value of the self diffusion coefficient of pure water. The value obtained in the present work is slightly less than that of pure water which may be accounted by the hydrophobic interaction between the noble gases and water.

4.5 Diffusion Coefficient as a function of temperature

In the previous section, we saw that the diffusion coefficient increases with increasing temperature. However, we didn't discuss the exact behavior of the dependence of the diffusion coefficient with temperature. In this section, we discuss that behavior. Like chemical reactions, diffusion is also a thermally activated process, as the kinetic energy of atoms and molecules increases with increase in temperature. This ultimately increases the velocity of the particles which governs the change in diffusion rate. The temperature dependence of diffusion appears in the form of an Arrhenius-type equation[11]

$$D = D_o \exp\left(-\frac{E_a N_A}{k_B T}\right) \qquad (12)$$

where D_o is the pre-exponential factor, N_A is the Avogadro number having value of 6.022×10^{23} per mole, and k_B is the Boltzmann constant having value equal to 1.38×10^{-23} J/K. E_a is the activation energy.

Rewriting *Equation 12* we get

$$\ln\left(\frac{D}{D_o}\right) = -\frac{E_a N_A}{k_B T} \qquad (13)$$

Thus a plot of ln(D) against 1/T should be a straight line if the diffusion coefficient follows Arrhenius behavior. *Figure 9* shows that Arrhenius behavior is followed by the diffusion coefficient. The experimental fit is obtained using values available in the literature.[2] The activation energy of xenon is 12.156 KJ/mole with MSD and 14.617 KJ/mole with VACF. The value of the activation energy is quite close to the experimental value of 12.8 KJ/mole.[3] Also the activation energy of the SPC/E water model has been estimated. The activation energy of water obtained with MSD in the present work is 14.69

KJ/mole, which is close to the experimental value of 16.927 KJ/mole.[17]

5. Conclusions

The diffusion coefficients obtained are quite close to the values reported by Jahne *et al.*[5] at 303 K and Weingartener *et al.*[3] at 323 K. The value of

the activation energies obtained with these parameters, 12.156 KJ/mole with MSD and 14.617 KJ/mole with VACF, are quite close to 12.8 KJ/mole obtained with the 129Xe NMR method.[3] The hydrophobic nature of xenon in the presence of water is confirmed via RDF analysis of xenon-xenon and oxygen-oxygen interaction.
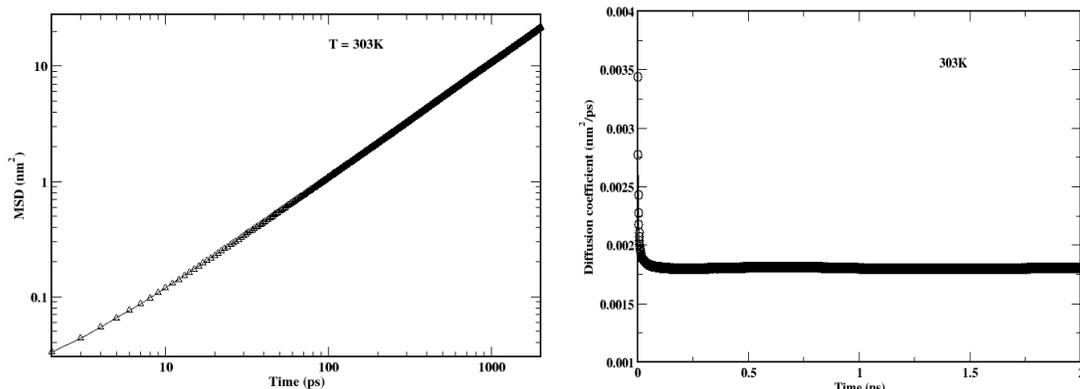

Figure 6. Logarithm plot of MSD vs time for xenon as a function of time at temperature 303 K in left and the plot of self-diffusion coefficient vs time in right at same temperature.
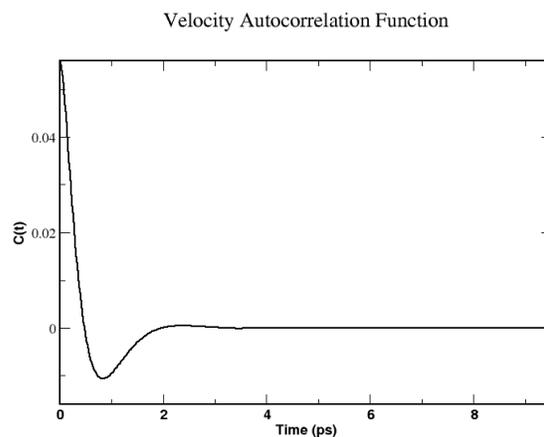
Figure 7. Variation of velocity auto-correlation function for xenon as a function of time at T=303K.

Table 6. Experimental and simulated values of the self-diffusion coefficient of Xe and the SPC/E model of water at different temperatures. D_{Xe} is the self-diffusion coefficient of xenon in water and D_{water} is that of water.

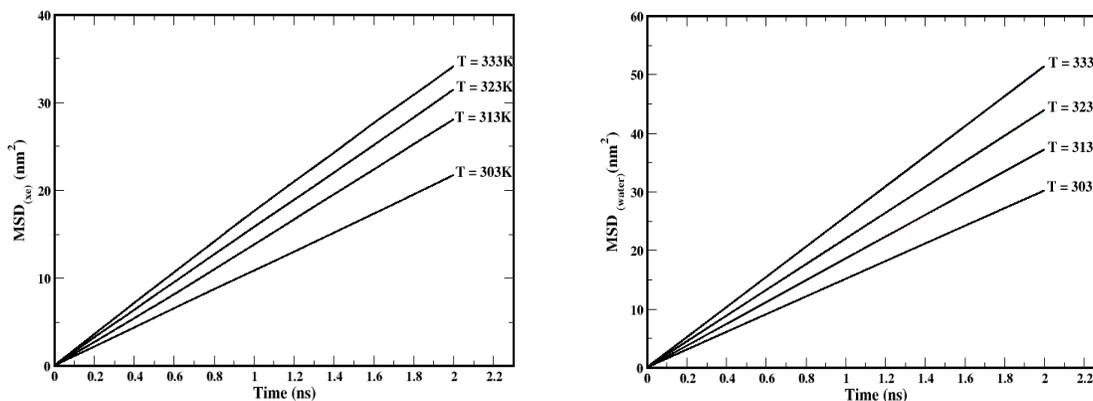| Temperature (K)	D_{Xe} ($\times 10^{-9} m^2 s^{-1}$)			D_{water} ($\times 10^{-9} m^2 s^{-1}$)	
	Experimental	Simulated		Experimental [17]	Simulated (MSD)
303	1.08 [2], 1.70 [5]	1.80	1.99	2.59	2.51
313	1.56 [2]	2.35	2.23	3.24	3.10
323	2.27[2],2.81[3]	2.61	2.89	3.97	3.65
333	3.98[2]	2.83	3.28	4.77	4.28

Figure 8. The MSD of xenon and water as a function of time at temperatures 303 K, 313 K, 323 K, and 333 K. The plot for xenon is on the left and that of water on the right.
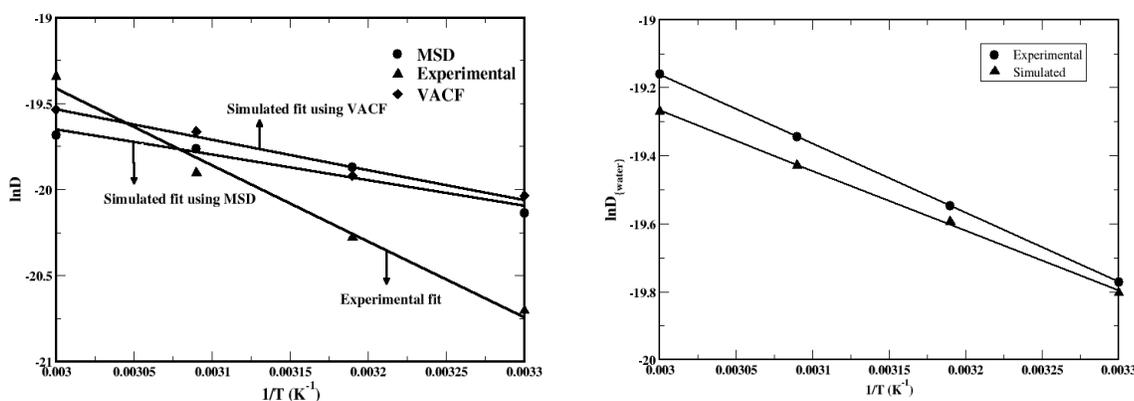

Figure 9. Comparison of an Arrhenius plot of the self-diffusion coefficients of Xe (left) and of water (right) with experimental fits. The experimental fits of xenon[2] and water[17] have been obtained by plotting values available in the literature.

References

[1] O. Coskuner and U. K. Deiters, *Z. Phys. Chem.*, **2007**, 221, 785.

[2] D. L. Wise and G. Houghton, *Chem. Eng. Sci.*, **1968**, 23, 1211.

[3] H. Weingartner, R. Haselmeier and M. Holz, *Chem. Phys. Lett.*, **1992**, 195 (5), 596.

[4] A. J. H. Boerboom and G. Klein, *J. Chem. Phys.*, **1969** 50, 1086.

[5] Jahne, B., Heinz, G., and Dietrich, W., *J. Geophys. Res.*, **1987**, 92, 10767.

[6] J. Wolber, S. J. Doran, M. O. Leach and A. Bifone, *Chem. Phys. Lett.*, **1998**, 296, 391.

[7] P. Heitjans and J. Krager, Diffusion in Condensed Matter: Methods, Materials, Models, **2009**, Springer, New York.

[8] J. Meller, Molecular Dynamics, **2001**, John Wiley & Sons, New York.

[9] J. Crank, The Mathematics of Diffusion, 2nd ed., **1975**, Oxford University Press, Oxford.

[10] H. Mehrer, Diffusion in Solids; Fundamentals, Methods, Materials, Diffusion-Controlled Processes, **2007**, Springer Series in Solid State Science, 155, Berlin.

[11] D. Frankel, B. Smit, Understanding Molecular Simulation From Algorithms to Applications, **2002**, Academic Press, USA.

[12] J.Vrabec, J. Stoll and H.Hasse, *J. Phys. Chem. B*, **2001**, 105, 12126.

[13] D. van der Spoel, E. Lindahl, B. Hess, A. R. van Buuren, E. Apol, P. J. Meulenhoff, D. P. Tieleman, A. L. T. M. Sijbers, K. A. Feenstra, R. van Drunen and H. J. C.

Berendsen, Gromacs User Manual version 4.5, **2010,** www.gromacs.org.

[14] H. J. C. Berendsen, J. R. Grigera and T. P. Straatsma, *J. Phys. Chem.*, **1987**, 91, 6269.

[15] P. Mark and L. Nilson, *J. Phys. Chem. A*, **2001**, 105, 9954.

[16] W. Humphrey, A. Dalke, and K. Schulten, *J. Molec. Graphics*, **1996**, 14, 33.

[17] A. J. Eastel, W. E. Price and L. A. Woolf, *J. Chem. Soc., Faraday Trans. 1*, **1989**, 15, 1091.